JOURNAL OF MATERIALS SCIENCE 23 (1988) 1064–1067

Physical and electrical properties of screen-printed $Zn_xCd_{1-x}S$ thick films

G. K. PADAM, V. SHANKER, P. K. GHOSH
Division of Materials, National Physical Laboratory, Hillside Road, New Delhi 110 012, India

Screen-printed thick films of $Zn_xCd_{1-x}S$ have been prepared in the entire composition range from pure CdS to pure ZnS and sintered at 800° C on alumina substrates. Their structural and electrical properties have been studied as a function of x. X-ray diffraction analysis of $Zn_xCd_{1-x}S$ established the presence of wurtzite structure for the range $0 \leqslant x \leqslant 0.8$, whereas for $x = 1.0$ the presence of the sphalerite structure of ZnS is observed. The lattice parameters a and c vary with x in accordance with Vegard's law. Scanning electron micrographs reveal an enhancement in porosity with increasing x. The dark electrical resistivity of the film increases with x in the range $0 \leqslant x \leqslant 0.6$, but beyond this range it starts decreasing. Photoconductivity is studied as a function of x. An effect of H_2 annealing on the dark resistivity and photosensitivity is established.

1. Introduction

$Zn_xCd_{1-x}S$ films are of considerable interest for heterojunction solar cells because their use in place of CdS permits a greater open-circuit voltage. The properties of polycrystalline $Zn_xCd_{1-x}S$ films produced by various methods like vacuum evaporation [1, 2], spray pyrolysis [3], reactive sputtering [4, 5] and chemical vapour deposition [6] for the purpose of reducing the production cost of heterojunction solar cells have been reported. However, the technique of screen printing and sintering, which is reported to be the cheapest and the most efficient way to produce CdS–CdTe heterojunction solar cells [7], has not so far been used for the preparation of $Zn_xCd_{1-x}S$ films.

In the present paper we report results obtained with $Zn_xCd_{1-x}S$ films prepared by the screen-printing technique in the entire composition range of $0 \leqslant x \leqslant 1.0$. We have compared structural, microstructural and electrical properties of the above films as a function of x.

2. Experimental details

Vacuum-grade CdS and ZnS powders were used in the present investigation. AR-grade $CdCl_2 \cdot H_2O$ and $ZnCl_2$ were used as fluxes. Slurries consisting of the CdS and ZnS powders in six different compositions corresponding to $x = 0.0$, 0.2, 0.4, 0.6, 0.8 and 1.0, $CdCl_2 \cdot H_2O$ (5 wt %), $ZnCl_2$ (5 wt %) and appropriate amounts of propylene glycol (binder) were prepared by mixing with a pestle and mortar. Each slurry was coated on an alumina substrate using an 80 mesh polyester screen and dried at 200° C for 2 h. A dried $Zn_xCd_{1-x}S$ film was then placed in a carbon case with a tight perforated cover (hole diameter = 1 mm, no. of holes = 12 per cm^2) and was sintered at 800° C in a nitrogen atmosphere with a flow rate of 4 l min^{-1}. Some of the samples were annealed in a hydrogen atmosphere at 200° C for 30 min in order to reduce the resistivity of the sintered $Zn_xCd_{1-x}S$ films.

These films were analysed for compositional, microstructural and structural properties by using energy-dispersive spectrometry (EDS) (Kevex 7000–77), SEM (JSM-35CF scanning electron microscope) and X-ray diffraction ($\lambda_{CuK\alpha} = 0.1541$ nm) techniques, respectively.

Electrical resistivity measurements were done in air at room temperature by using a 610 C Keithley electrometer. Air-drying silver paste was used for contacts. Resistance measurements were made in the dark (after a stable state has been reached) and in the light provided by a tungsten lamp. All the measurements in light were made at a constant intensity of 38 mW cm^{-2}. The type of conductivity of the $Zn_xCd_{1-x}S$ films was determined by the hot-probe method. The film thickness was measured by using a scanning electron microscope.

3. Results and discussion

Strongly adherent $Zn_xCd_{1-x}S$ films were obtained throughout the composition range, with the colour gradually varying from bright yellow for CdS to white for ZnS. Films in the thickness range of 25 to 30 μm were obtained.

3.1. Composition of sintered screen-printed $Zn_xCd_{1-x}S$ films

The variation of the film composition (x_{film}) is illustrated in Fig. 1 as a function of x_{slurry}. It shows that the film contains relatively more zinc than the slurry.

Several authors have reported differences between the compositions of initial and final phases of ZnCdS films produced by a spray technique, depending upon the substrate temperature. At lower substrate temperatures (200° C), Reshamwala *et al.* [8] reported an equality of composition on the basis of atomic absorption analysis. However, Duchemin *et al.* [9] observed an enrichment in zinc in the ZnCdS film deposited at 600° C by the same spray-pyrolysis tech-

0022–2461/88 $03.00 + .12

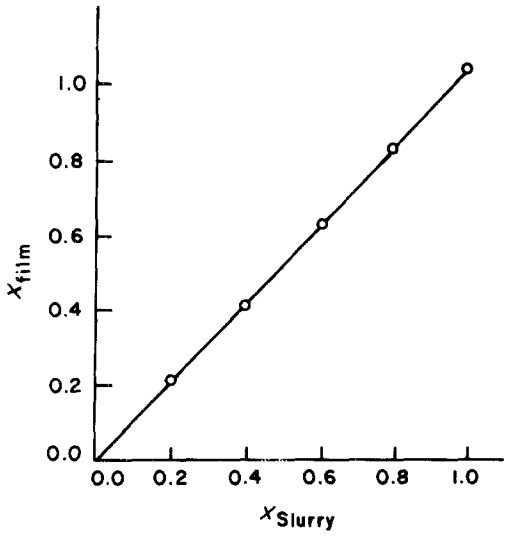

Figure 1 Zinc concentration in the film against that in the slurry.

nique. Since in the present case the screen-printed films are sintered at the still higher temperatures of 800° C, it is very probable that the observed excess of zinc sulphide is due to the higher volatility of cadmium sulphide. Similar observations were also made by Dachraoui and Vedel [10] in the case of spray-deposited ZnCdS thin films.

3.2. Crystal structural properties

X-ray diffraction (XRD) analysis showed that the alloy films of CdS and ZnS exist in single-phase wurtzite or sphalerite, depending upon the composition, and therefore the two materials form a solid solution in the entire composition range $0 \leqslant x \leqslant 1.0$. Wurtzite structure in the polycrystalline $Zn_xCd_{1-x}S$ films was observed in the range $0 \leqslant x \leqslant 0.8$, whereas films with $x = 1.0$ possess the sphalerite structure of ZnS. To ascertain that the films were homogeneously alloyed, diffraction patterns were taken from different regions and a slight change in the lattice parameters was observed.

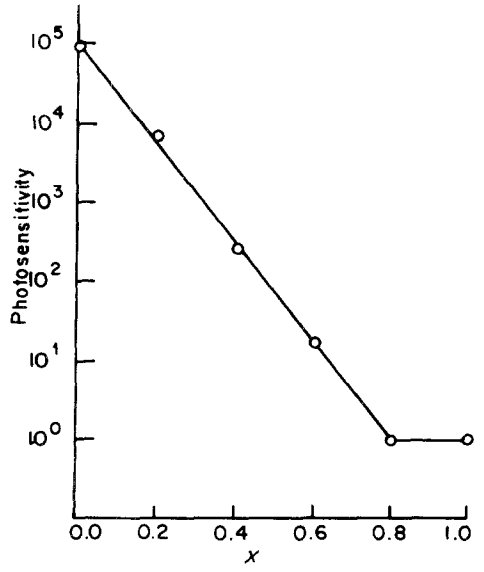

Figure 2 Variation of lattice parameters a and c of $Zn_xCd_{1-x}S$ solid solutions.

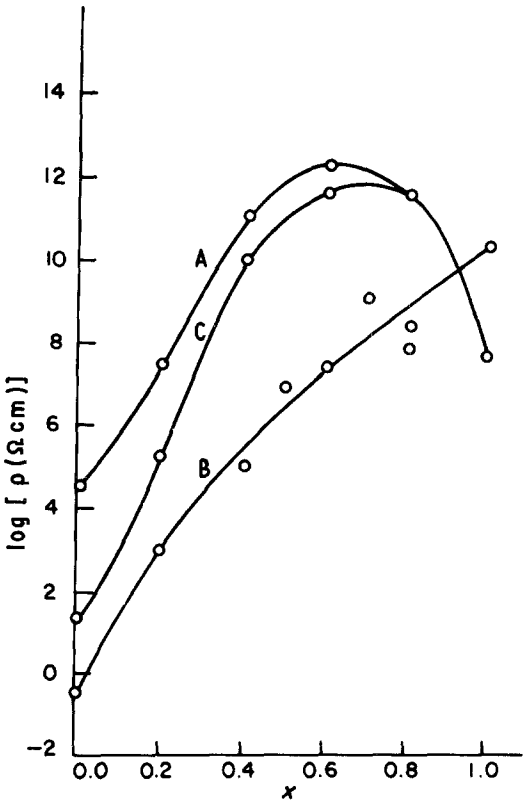

Figure 3 Variation with x of intensity of X-ray diffraction lines (1 0 0), (1 0 1) and (1 0 2) belonging to zinc.

Lattice constants a and c of the films are plotted as a function of x in Fig. 2. A continuous variation of lattice parameters with composition is observed, obeying Vegard's law, but the values of a and c are lower than those reported by Cherin *et al.* [11] for single crystals. The relations between the lattice parameters (measured in nanometres) and the composition may be expressed as

$$a = 0.4129 - 0.0345x \quad \text{(this work)} \quad (1)$$

$$a = 0.4137 - 0.0316x \quad \text{(Cherin } et\ al.\text{)} \quad (2)$$

and

$$c = 0.6716 - 0.0580x \quad \text{(this work)} \quad (3)$$

$$c = 0.6717 - 0.0460x \quad \text{(Cherin } et\ al.\text{)} \quad (4)$$

The lattice parameter a of $Zn_xCd_{1-x}S$ ($x = 1.0$) film was also determined by X-ray analysis and found to be 0.541 nm, which is in good agreement with the calculated lattice parameter value 0.540 nm of ZnS bulk material (ASTM Card No. 5-566).

Apart from the diffraction lines of alloyed $Zn_xCd_{1-x}S$ films, three additional diffraction lines with d (nm) = 0.229 (1 0 0), 0.209 (1 0 1) and 0.166 (1 0 2) start appearing at $x = 0.6$ and their intensity increases with x, as shown in Fig. 3. These three lines have been identified as zinc lines when compared with ASTM Card No. 4-831 for metallic zinc.

3.3. Microstructural properties

The SEM photographs of three $Zn_xCd_{1-x}S$ films of a similar thickness ($\sim 25\,\mu m$) with $x = 0$, 0.2 and 1.0 are shown in Figs 4a, b and c, respectively. As

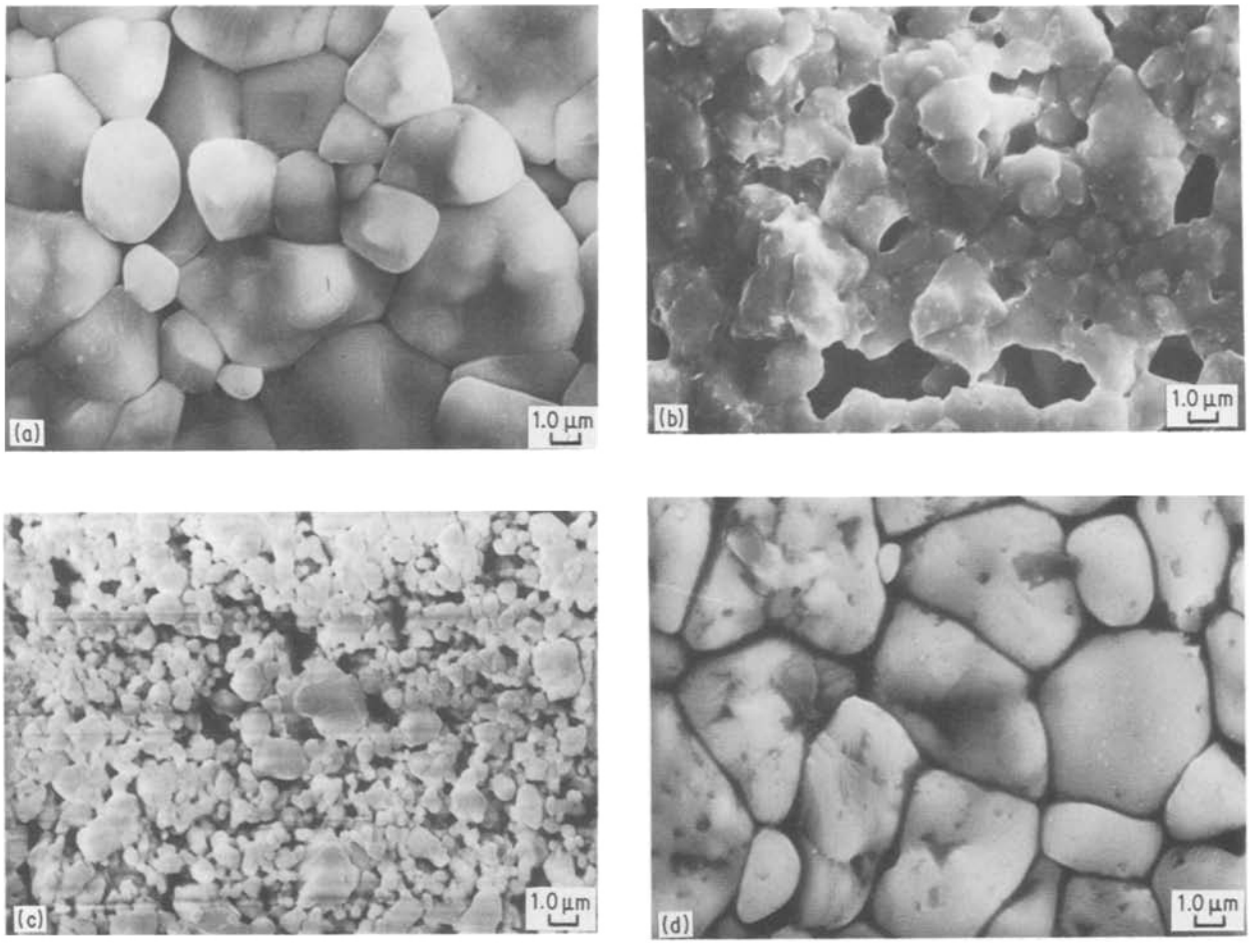

Figure 4 Scanning electron micrographs of screen-printed films sintered at 800° C for 30 min in N_2 atmosphere for (a) $x = 0$, (b) $x = 0.2$ and (c) $x = 1.0$. (d) Film (a) annealed in H_2 at 200° C for 30 min.

observed, the films with added ZnS were more porous and the grains were also less uniform.

The grain size decreased with increasing x. At $x = 0$ the average grain size is 3.7 μm (Fig. 4a), at $x = 0.2$ the average grain size is 1.0 μm (Fig. 4b), and at $x = 1.0$ the average grain size is 1.0 μm (Fig. 4c). Similar results have also been observed in $Zn_xCd_{1-x}S$ thin films [12]. On annealing in an H_2 atmosphere at 200° C for 30 min, the average grain size increased from 3.7 to 5.5 μm and the surface seemed to be more coherent and many hexagonal crystallites appeared (Fig. 4d). The more regular morphology provides the fact that H_2 annealing makes the structure of screen-printed films to be more stable.

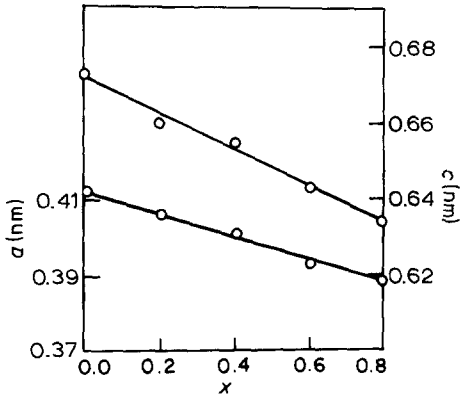

Figure 5 Variation of logarithm of resistivity ϱ with x for (A) screen-printed and sintered film of $Zn_xCd_{1-x}S$, (B) vacuum-evaporated $Zn_xCd_{1-x}S$ thin film [1], and (C) Film (A) annealed in H_2 at 200° C for 30 min.

3.4. Electrical properties

The type of conductivity of the $Zn_xCd_{1-x}S$ films was examined by the hot-probe method and all the films were found to be n-type in the entire range of $0 \leqslant x \leqslant 1.0$.

For electrical resistivity measurements, the $Zn_xCd_{1-x}S$ films when placed in the dark took a long time to achieve a stable dark resistance, sometimes many hours, indicating the presence of many trapping centres. Resistivity measurements were not made until a stable state was reached. This type of behaviour was predominant for lower values of x and the $Zn_xCd_{1-x}S$ films for higher values of x were not affected by the environment.

The dark electrical resistivity (ϱ) variation as a function of x is shown in Fig. 5. It is seen that the resistivity of the films increases from 3×10^4 to $3 \times 10^{12}\,\Omega$cm with x in the range of $0 \leqslant x \leqslant 0.6$ (curve A). However, beyond this region the resistivity decreases. In the present case of sintered screen-printed films of $Zn_xCd_{1-x}S$, the resistivity behaves in a fashion similar to that of spray-deposited [3] and vacuum-evaporated $Zn_xCd_{1-x}S$ thin films [1] only up to a value of $x = 0.6$. Beyond this value of x ($\geqslant 0.6$) the resistivity shows a decrease, contrary to the observations made in thin films. For comparison, the

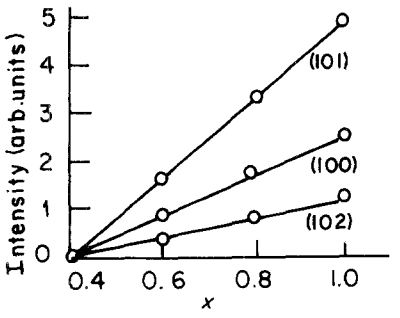

Figure 6 Photosensitivity (photoconductivity/dark conductivity) against x for Zn_xCd_{1-x} films.

variation of resistivity with x in the case of evaporated $Zn_xCd_{1-x}S$ films [1] is shown in curve B of Fig. 5. An initial increase in resistivity may be attributed to the increase in the band-gap of the solid solution with increasing percentage of ZnS in CdS. However, further increase of ZnS percentage may lead to an excess of zinc either in the lattice or as a separate phase which may be responsible for a subsequent decrease in ϱ beyond $x = 0.6$. As mentioned earlier (Section 3.2), the XRD patterns of $Zn_xCd_{1-x}S$ films with $x \geqslant 0.6$ show the presence of metallic zinc along with the wurtzite/sphalerite $Zn_xCd_{1-x}S$ phase. Also, the intensity of these zinc lines increases with increasing x. Therefore, the possibility of excess zinc in the lattice contributing to the lowering of resistivity may be ruled out. Instead, the decrease in the value of ϱ beyond $x = 0.6$ can be ascribed to the metallic zinc present as a separate phase in $Zn_xCd_{1-x}S$ films.

The high resistivity observed in the present case could be due to oxygen adsorption. In polycrystalline CdS, electrical conduction is dominated by grain boundary scattering, oxygen chemisorption and the electronic effect of chemisorption on the grain boundaries [13]. In contrast to CdS films, the resistivity of ZnS films in insensitive to oxygen. Since annealing in an H_2 atmosphere is more effective in reducing the resistivity of CdS than annealing in other atmospheres such as H_2 or argon [14], sintered $Zn_xCd_{1-x}S$ films were annealed in H_2 at 200° C for 30 min. It was found that the resistivity of $Zn_xCd_{1-x}S$ films reduced from 3×10^4 to 20 Ω cm and from 3×10^7 to 2×10^5 Ω cm for $x = 0$ and $x = 0.2$, respectively. For a further increase of x, the decrease in resistivity value is small and for $x = 0.8$ and 1.0 no change in resistivity is observed after H_2 annealing. Results are shown in curve C of Fig. 5.

The photoconductivity of the $Zn_xCd_{1-x}S$ films was also measured and Fig. 6 shows the variation with x of photosensitivity (photoconductivity/dark conductivity) of $Zn_xCd_{1-x}S$ films. It is clear from the figure that even a very small addition of ZnS in CdS reduces the photosensitivity drastically from 10^5 for pure CdS to 1 for pure ZnS.

Photoconductivity in screen-printed CdS films has been observed by Fu *et al.* [15] and Amalnerkar *et al.* [16]. Fu *et al.* reported that the photoconductivity phenomenon is associated with the complex defect centre $V_{Cd}Cl_S$, whereas in the work of Amalnerkar *et al.* [16] the photoconductivity is correlated with oxygen chemisorbed on the surface of screen-printed CdS films. In the present case of sintered screen-printed $Zn_xCd_{1-x}S$ (for lower values of x), the cause of appearance of photoconductivity could also be associated with the acceptor-like states formed by chemisorbed oxygen. To examine the role of oxygen in the photoconductivity behaviour of the films, the films were annealed in H_2. It was observed that H_2 annealing leads to the quenching of photosensitivity in all the films. As mentioned earlier, the decrease in dark resistivity upon H_2 annealing is possibly associated with the removal of oxygen. Therefore, the quenching of photosensitivity can be attributed to a decrease in the number of acceptor-like oxygen states upon H_2 annealing. Pure ZnS shows no change in resistivity on H_2 annealing, indicating an absence of oxygen states. The initial high dark resistivity before H_2 annealing of CdS and CdS-rich films is clearly due to compensation caused by the acceptor-like oxygen states. The photoconductivity behaviour of the present sintered screen-printed $Zn_xCd_{1-x}S$ films is similar to that of spray-deposited $Zn_xCd_{1-x}S$ thin films [3].

The technique of screen printing provides a simple means of preparing films of $Zn_xCd_{1-x}S$, the properties of which can be tailored by changing the relative contents of the individual materials.

Acknowledgements

The authors are thankful to Mr D. K. Suri, Mr S. U. M. Rao and Dr M. N. K. Kamalsanan for taking XRD patterns, SEM and photoconductivity measurements, respectively.

References

1. L. C. BURTON and T. L. HENCH, *Appl. Phys. Lett.* **29** (1976) 612.
2. V. D. VANKAR, S. R. DAS, PREM NATH and K. L. CHOPRA, *Phys. Status Solidi (a)* **45** (1978) 665.
3. A. BANERJEE, PREM NATH, V. D. VANKAR and K. L. CHOPRA, *ibid.* **46** (1978) 723.
4. R. J. ROBINSON and Z. K. KUN, *Appl. Phys. Lett.* **27** (1975) 74.
5. S. DURAND, *Thin Solid Films* **44** (1977) 43.
6. T. M. RAZYKOV, *Solar Energy Mater.* **12** (1985) 233.
7. H. MATSUMOTO, K. KURIBAYASHI, H. UDA, Y. KOMATSU, A. NAKUNO and S. IKEGAMI, *Solar Cells* **11** (1984) 367.
8. N. A. RESHAMWALA, W. B. HSU and L. C. BURTON, in Proceedings of European Photovoltaic Solar Energy Conference, Cannes, 1980, p. 787.
9. S. DUCHEMIN, M. KAKA, I. YOUM, BOUGNOT and M. CADENE, in Proceedings of Seminaire Surles Cellules Solaires CdS–CuS, Montpelier, July 1983.
10. M. DACHRAOUI and J. VEDEL, *Solar Cells* **15** (1985) 319.
11. P. CHERIN, E. L. LIND and E. A. DAVIS, *J. Electrochem. Soc.* **117** (1970) 233.
12. H. L. HWOK, *J. Phys. D, Appl. Phys.* **16** (1983) 2367.
13. K. L. CHOPRA, R. C. KAINTHLA, D. K. PANDYA and A. P. THAKOOR, *Phys. Thin Films* **12** (1982) 167.
14. R. R. CHAMBERLIN and R. S. SKARMAN, *J. Electrochem. Soc.* **113** (1986) 86.
15. SHEN-LI FU, TIEN-SHOU WU and MAU-PHON HOUNG, *Solar Energy Mater.* **12** (1985) 309.
16. D. P. AMALNERKAR, M. S. SETTY, N. R. PAVASKAR and A. P. B. SINHA, *Bull. Mater. Sci.* **2** (1980) 251.

Received 1 June
and accepted 27 July 1987